İSTANBUL UNIVERSITY CERRAHPAŞA

ORIGINAL ARTICLE
Electrica 2022; 22(2): 301-312

Performance Analysis of Boost-Converter-Fed BLDC Motor Drive with Motoring and Braking Operation for Electric Rickshaw Application

Rajendiran Amalrajan, Ramachandiran Gunabalan

Vellore Institute of Technology, School of Electrical Engineering – Chennai, Tamil Nadu, India

Cite this article as: R. Amalrajan and R. Gunabalan, "Performance analysis of boost-converter-Fed BLDC motor drive with motoring and braking operation for electric rickshaw application," *Electrica.,* 22(2), 301-312, 2022.

ABSTRACT

Electrical vehicle technology offers promising solutions to ensure fuel saving and emission reductions. A brushless DC (BLDC) motor drive in the electric rickshaw is the most attractive in the current scenario, due to the inherent operation of the motor in the forward and reverse directions. In this paper, a 48 V, 1 kW BLDC motor drive with a DC generator loading arrangement is tested under different running conditions, and the speed, power, and torque characteristics are presented. A DC–DC boost converter is introduced in the system in order to minimize the voltage rating and size of the battery source. The boost converter with dSPACE controller maintains a 48 V DC-link voltage, irrespective of battery voltage conditions, in closed-loop control. The proportional-integral (PI) control for the boost converter is constructed in the MATLAB environment and provides a control signal to the power electronics switches through the dSPACE controller. There are no additional circuits for the PI controller in the boost converter. The simulation is performed in the MATLAB environment with 24 V battery, a boost converter, and a 1 kW BLDC motor drive. An experimental setup is provided with a dSPACE controller, and the results are presented, to validate the effectiveness of the drive system in forward and reverse motoring. The overall efficiency of the drive system is 83% at rated condition.

Index Terms—Brushless DC (BLDC) motor, DC–DC converter, dSPACE controller, electric vehicle, torque sensor.

I. INTRODUCTION

One of the major consumers of fossil fuels is the transportation sector. Electric vehicles (EVs) minimize the limitations of fossil fuels and are preferred for pollution-free transportation. They employ battery banks, power electronic converters, and controllers to drive the electric motor, which makes them eco-friendly and zero-emission vehicles. The brushless DC (BLDC) motor, the permanent magnet synchronous motor (PMSM), and the induction motor (IM) are used in EVs. The BLDC motor is used for low-power two-wheel and three-wheel EV applications, and the IM is preferred for heavy-duty EV applications. Plug-in EV/hybrid vehicle design and development is adopted worldwide. The developers are Nissan Leaf, BMW, Tesla, Audi, Jaguar, Hyundai, Volkswagen, Renault, Infiniti, Rivian, Polestar, etc. The popularity of EV design and development has increased in recent years due to government subsidies, with increased battery range, low cost, and minimum cost to the environment [1].

During the motoring mode, the energy is utilized from the battery source to activate the drive system. During frictional or mechanical braking mode, the kinetic energy of the drive system is wasted as heat energy. To minimze the energy losses and to improve efficiency, regenerative braking is employed in EVs. Regenerative braking is used to feed energy while braking, when the inertia forces the motor into generator mode, and can increase the range of travel distance. When the battery is 100% charged, the regenerative braking energy cannot be stored. In this case, effective braking is possible when the energy is stored in some other energy storage devices. During acceleration, EVs (IM, PMSM, and BLDC) require low voltage and high current, supplied by the battery. The electrical energy discharged during acceleration is directly proportional to the starting current drawn by the electric motor, with respect to time. The continuous operation of EVs reduces the battery life cycle. The limitations of the battery are the inefficient utilization of energy during a short period and system failure due to overcurrent. A supercapacitor (ultracapacitor) is an alternative energy storage device for maximum energy restoration (charging) of batteries. The use of a battery [2, 3] with an auxiliary energy system was found to add to the cost and design

Corresponding Author:
Ramachandiran Gunabalan

E-mail: gunabalan.r@vit.ac.in

Received: July 27, 2021

Revised: October 28, 2021

Accepted: December 11, 2021

Available Online Date: April 5, 2022

DOI: 10.54614/electrica.2022.21093

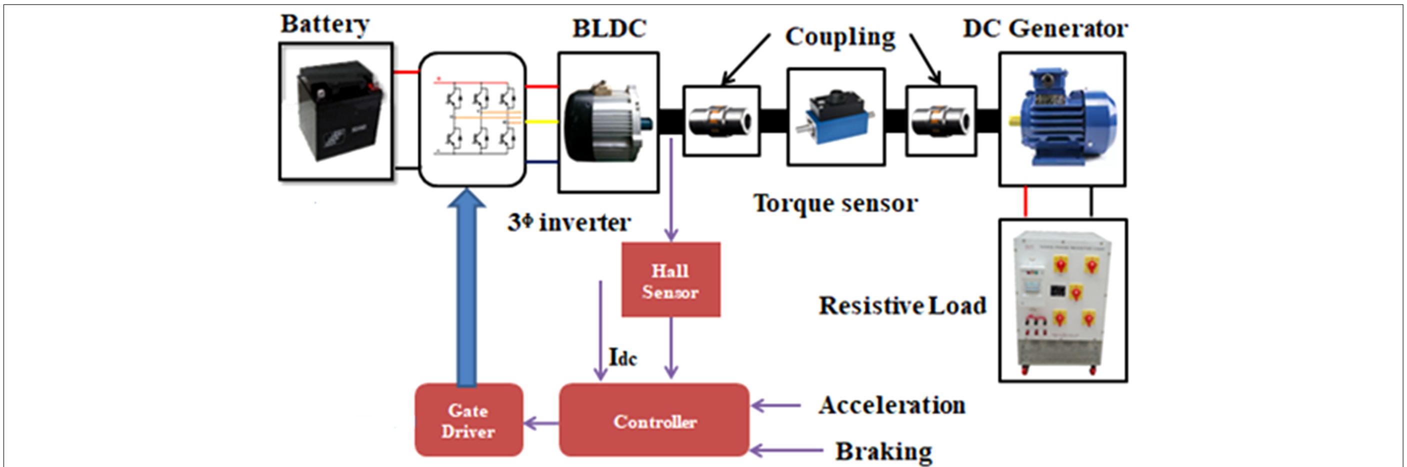

Fig. 1. Block diagram of BLDC motor drive with controller.

complexity, though the energy was effectively utilized. However, the bi-directional DC–DC converter with higher rating decreases the efficiency of regenerative braking. In [4, 5], a cascaded converter was used to utilize the energy from the supercapacitor effectively. The cascaded converter was operated in a bidirectional mode, which increases the overall cost. In order to increase the flexibility and better functionality, multi-parallel-connected DC–DC converters were used [5-7]. These converters require a single passive component that increases the efficiency of the system [8, 9]. Moreover, the overall weight and volume were decreased. The cost of the system was greatly increased, as was the complexity of design of the DC–DC converter, whereas the selection of the ultracapacitor needs to be addressed to minimize the cost of the overall system. The limitation in multi parallel and cascaded bidirectional DC–DC converter was overcome by using the multi-mode single converter [10].

The power circuit is necessary to control the motor drive, with suitable techniques for chopper control. Two-quadrant chopper control is particularly preferred, in which quadrant 1 is used during acceleration for traction, and quadrant 4 is used during regenerative mode of operation [11-14]. The anti-braking system or the fully electrified regenerative braking system (FE-RBS) is employed for performance improvement. During braking, the FE-RBS is used to restore the energy in the battery and supercapacitor [15-17]. EV control techniques, and controllers such as conventional linear quadratic control, artificial neural network, fuzzy logic, electro hydraulic brake system, current amplitude modulation, and stochastic dynamic programming are discussed in [18, 19]. To increase the efficiency under regenerative braking, the low-speed region was identified and verified in the hardware in loop [20]. Pneumatic pressure control was used for the regenerative brake mechanism in trucks [21]. The vehicle dynamics were studied in MATLAB for a known vehicle drive cycle. The regenerative braking system for a four-wheel EV under fixed and variable braking strength was simulated, without compromising efficiency and stability [22, 23]. The anti-lock braking system was coordinated with the regenerative braking system to enhance the efficiency of the braking energy [24].

The role of the DC–DC converter is very vital for regenerative braking in EV technology, for feeding the energy back to the source. This energy is stored in power back-up devices, like the battery, during braking. In the present scenario, an efficient regenerative braking system with battery safety and improved vehicle acceleration is needed. The purpose of the DC–DC converter is to provide maximum energy transfer to the battery and enable the smooth functioning of the system. The selection of the DC–DC converter depends on the drive applications. The design lowered the system's complexity and cost, and increased the overall system efficiency. In this paper, the performance analysis of the inverter and the DC–DC converter-fed BLDC drive system is discussed in detail for clear understanding. A DC shunt generator is coupled with the motor, and the results are presented for different electrical load conditions.

Section II discusses the inverter-fed BLDC motor drive with a DC generator loading arrangement, where the performance of the motor is tested under forward- and reverse-motoring modes under different running conditions.

Section III discusses the boost-converter-embedded BLDC motor drive with a DC generator loading arrangement, where the performance of the motor is tested under forward- and reverse-motoring modes under different running conditions.

II. INVERTER-FED BLDC MOTOR DRIVE WITH LOADING ARRANGEMENT

The block diagram shown in Fig. 1 consists of a BLDC motor, a DC generator, a mechanical coupler, a torque sensor, an electrical loading arrangement, and a battery. A 48 V DC supply is derived from a lithium ion phospate battery ($LiFePO_4$). It has longer life span, less weight, no maintenance, and high charging and discharging efficiency. The DC supply is fed to the three-phase trapezoidal inverter and its output AC supply drives the BLDC motor. The feedback signal of the Hall sensor is given to the BLDC controller to generate the required control signal for the power electronic inverter. The BLDC motor shaft is coupled with the primary end of the torque sensor and the secondary end of the torque sensor is coupled with the DC generator. The shaft coupler's dimensions are selected as per the shaft dimensions of the BLDC motor, torque sensor, and DC generator. The excitation of the DC generator is adjusted to obtain the rated voltage of 220 V at the rated field current. A resistive load of 1 kW is connected to the DC generator for electrical loading. The circuit consists of the inverter, the gate driver, and the controller of the BLDC motor drive with battery, shown in Fig. 2. The ratings and the specifications of the battery and the motor are listed in Table I.

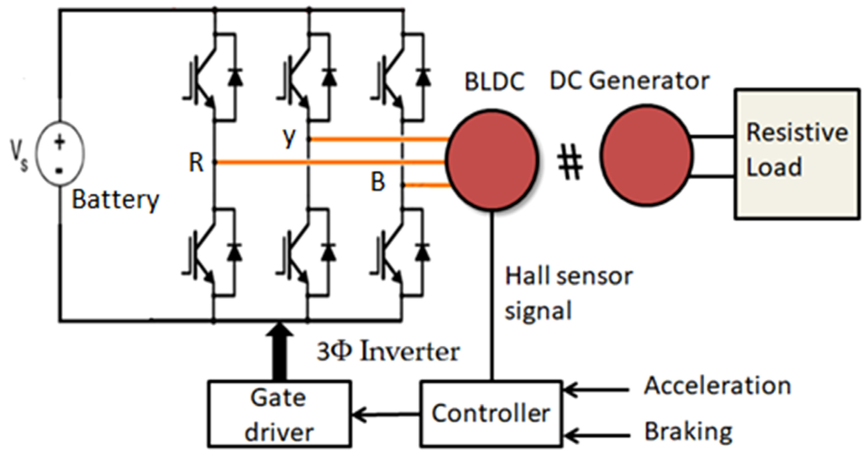

Fig. 2. Circuit diagram of the BLDC motor drive with controller.

The stall current and stall torque of the BLDC motor are calculated using the following standard equations [11]:

$$\text{Motor equation}: V = E + RI \tag{1}$$

$$\text{Speed equation}: \omega = \left[1 - \frac{T}{T_0}\right] \tag{2}$$

$$\text{No load speed } \omega_0 = \frac{V}{k} \tag{3}$$

For a 48 V BLDC motor with a rated speed of 3000 rpm, the torque constant is calculated as follows:

$$k = \frac{V}{\omega_0} = \frac{V}{2\pi N / 60} = \frac{V * 60}{2\pi N} \tag{4}$$

The stall current of the motor is

$$I_0 = V / R \tag{5}$$

The stall torque of the motor is

$$T_0 = kI_0 \tag{6}$$

TABLE I. SPECIFICATIONS OF THE BLDC MOTOR SETUP

Specifications	
Lithium-ion phosphate battery	48 V, 24 Ah
Inverter switch	50 A, 200 V
BLDC motor	48 V, 1000 W, 3000 rpm, 8 pole
Lorenz USB torque sensor	15000 rpm, 200 Nm
DC generator	220 V, 1500 rpm, 1000 W
Torque constant k	0.153 V/(rad/s)
Stall torque T_o	3.06 Nm
Boost converter input supply voltage	24 V
Inductor	1.5 mH, 40 A
Capacitor	200 V, 670 μF
MOSFET [IRFP4332PBF]	200 V, 40 A
POWER diode [MUR3060]	30 A
Switching frequency	20 kHz

A. Forward and Reverse Motoring on the Inverter-Fed BLDC Drive

The performance of the BLDC drive is determined under forward and reverse motoring at different load conditions. The prototype experimental arrangement for a 1 kW BLDC drive with hand throttle control is shown in Fig. 3. A DC generator is coupled with the motor through the Lorenz USB torque sensor, which measures the torque under different load conditions. Aluminum coupling with suitable dimensions is provided at both ends of the torque sensor to couple the BLDC motor and DC generator. The switching pulse of the inverter is generated by the controller, and the switching frequency at rated speed is 3 kHz. MOSFET switches are used to build the power circuit. The timing frequency at the rated speed of 3000 rpm is 200 Hz. The switching pulse at the rated running condition is illustrated in Fig. 4(a). It is inferred from the figure that the switching frequency of the inverter is 3 kHz. The output voltage corresponds to 3000 rpm, shown in Fig. 4(b). The corresponding timing frequency is 20 Hz, and it varies with respect to the speed.

The DC supply voltage and current, the inverter line voltage, and the line current of the BLDC motor are observed at no load, 250 W, 500 W, and 750 W. The values are presented in Tables II and III, for forward and reverse motoring respectively. The input and the output power are calculated using the following equations:

$$\text{Efficiency} = \frac{\text{Output power}}{\text{Input power}} \tag{7}$$

$$\text{Input power} = \text{Battery output} = V_{bat} \times I_{bat} \tag{8}$$

$$\text{Output power} = \text{Generator output} = V_G \times I_G \tag{9}$$

The output voltage and current waveforms captured at different load conditions are illustrated in Fig. 5. Both simulation and experimental results are presented, in order to validate the performance of the drive system. The simulation model for the drive is constructed by the various blocksets available in Simulink in MATLAB. Fig. 5(a) shows the no-load waveforms of both input and output

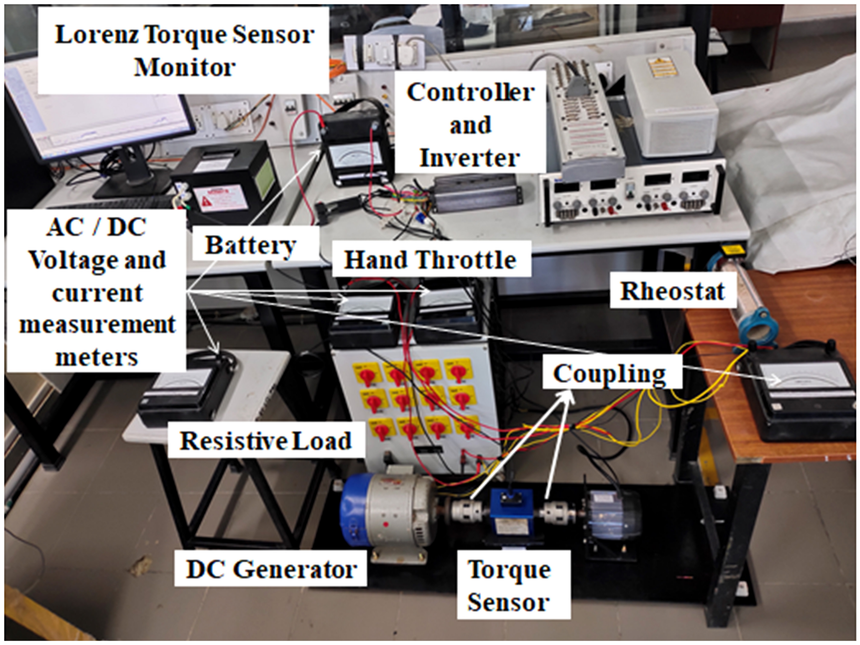

Fig. 3. Experimental setup to perform load test on BLDC.

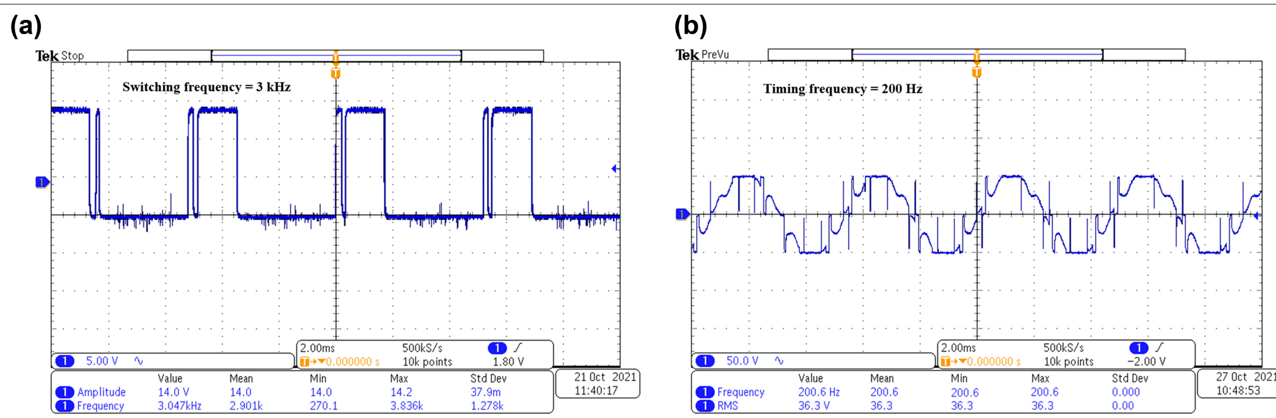

Fig. 4. (a) Switching pulse at rated operating condition. (b) Output voltage waveform at 3000 rpm.

voltage and current. The DC input supply voltage is 48.12 V and the current is 3.41 A. The output no-load current is 3.4 A, and the line voltage is 24.26 V at a speed of 1463 rpm. Fig. 5(b) and (c) shows the load voltage and current waveforms at 250 W and 500 W respectively. The Hall effect sensor detects the position of the rotor. The output signals of the Hall sensors are captured by MSO, as shown in Fig. 5(d). The signal is a square wave with 120^0 electrical. The amplitude of the control signal is 5 V, which is amplified by the driver circuit in order to switch on the power electronics switches in the converter.

TABLE II. FORWARD-MOTORING CHARACTERISTICS

DC Supply		BLDC		DC Generator					
Input Voltage (V)	Input Current (A)	Line Voltage (V)	Line Current (A)	Field Current (A)	Load Current (A)	Load Voltage (V)	Speed (rpm)	Resistive Load (W)	Torque (Nm)
48.3	3.4	24.26	5.7	0	0	16	1463	0	0
48.3	8.9	24.83	10.1	0.24	1.77	200	1475	250	2.23
48.3	12.3	25.91	13.2	0.24	2.68	185	1460	500	3.24
48.3	13.5	26.96	14.1	0.24	3.12	175	1472	750	3.56

TABLE III. REVERSE-MOTORING CHARACTERISTICS

DC Supply		BLDC		DC Generator					
Input Voltage (V)	Input Current (A)	Line Voltage (V)	Line Current (A)	Field Current (A)	Load Current (A)	Load Voltage (V)	Speed (rpm)	Resistive Load (W)	Torque (Nm)
48.3	2.9	22.54	4.9	0	0	16	−1463	0	0
48.3	4.8	22.43	6.5	0.24	1.32	145	−1475	250	−1.2
48.3	6.3	22.23	8.2	0.24	1.92	132	−1460	500	−1.6
48.3	7	21.80	8.6	0.24	2.3	122	−1472	750	−1.69

B. Power, Torque, and Speed Characteristics

Different performance parameters like torque, speed, and power are plotted with Lorenz USB torque sensor data, which are stored in the desktop. The DC generator is loaded gradually and the corresponding speed, torque, and power values are measured by the torque sensor. The power, torque, and speed characteristics with respect to time under forward and reverse motoring are shown in Fig. 6(a) and (b), respectively. For the forward-motoring operation, the motor runs at 1477 rpm at different load conditions. The power, torque, and speed for 2.23 Nm (250 W), 3.24 Nm (500 W), and 3.56 Nm (750 W) are

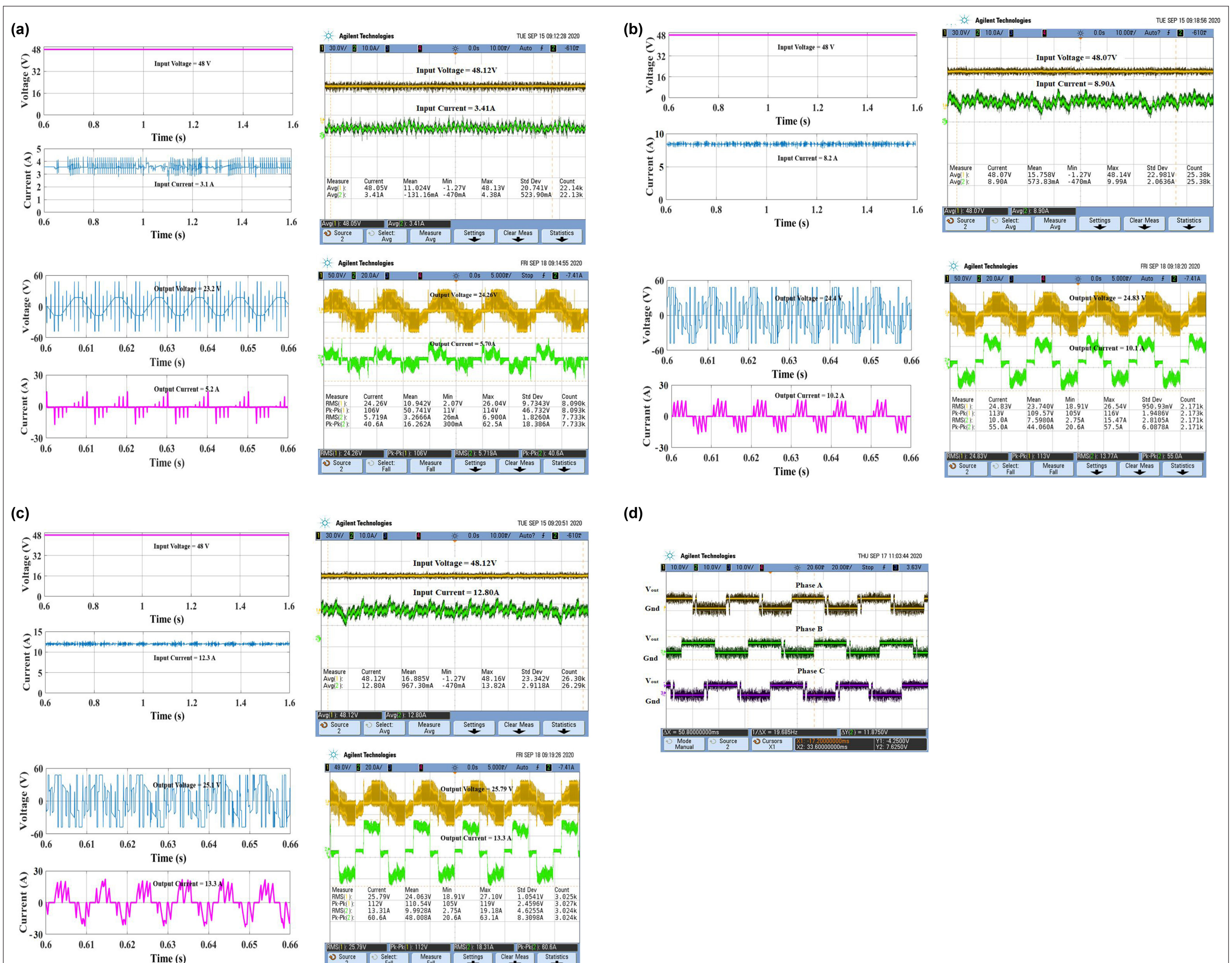

Fig. 5. Voltage and current waveforms at different load conditions. (a) Waveforms at no-load condition. (b) Waveforms at 2.23 Nm load condition. (c) Waveforms at 3.24 Nm load condition. (d) Hall effect sensor signal.

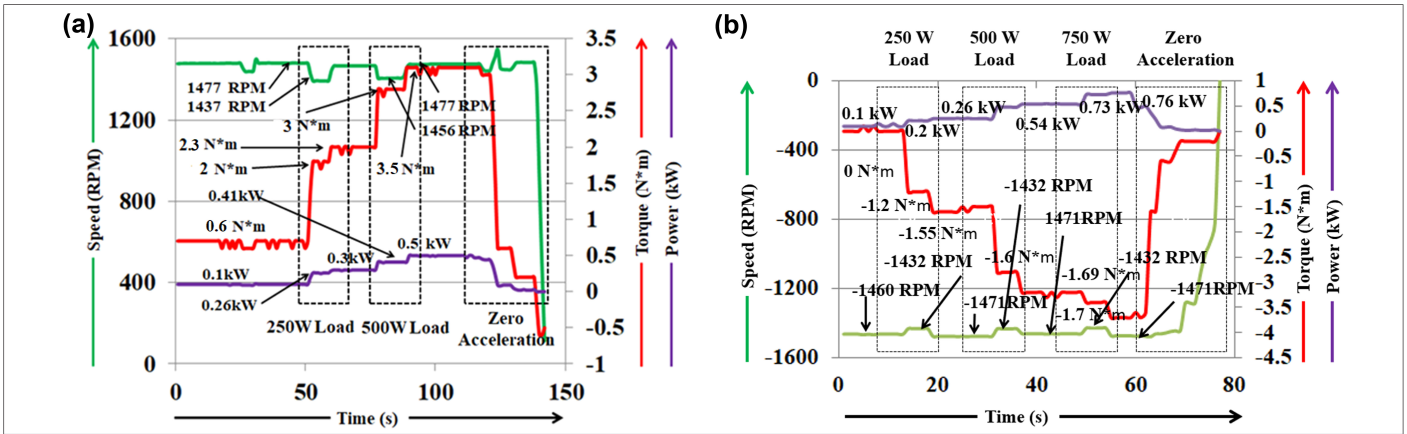

Fig. 6. (a) Forward-motoring speed, torque, and power characteristics. (b) Reverse-motoring speed, torque, and power characteristics.

observed and plotted. For the reverse-motoring operation, the motor runs at −1463 rpm at different load conditions. The power, torque, and speed for −1.2 Nm (250 W), −1.6 Nm (500 W), and −1.69 Nm (750 W) are observed and plotted. It is observed that in both forward and reverse motoring, the speed is maintained constant under different torque levels, and speed dip is observed for a short period. The overall efficiency of the drive system is calculated by measuring battery output power (inverter input) and generator output power, and the values are provided in Table IV. The average system efficiency is 83.6%.

TABLE IV. EFFICIENCY OF THE INVERTER-FED DRIVE SYSTEM

Battery Power (W)	BLDC Output Power (W)	Generator Power (W)	Overall Efficiency (%)
Forward Motoring			
425.04	344.44	354	83.29
594.09	500.45	495.8	83.48
652.05	550.45	546	83.73
Reverse Motoring			
231	185.35	191.4	82.85
304	244.62	253.44	83.36
338	260.50	280.6	83.01

III. BOOST-CONVERTER-FED BLDC MOTOR DRIVE WITH LOADING ARRANGEMENT

The block diagram of a BLDC drive with DC–DC boost converter is shown in Fig. 7. The switch operates under high switching frequency (20 kHz) and helps in generation of a constant voltage from the boost converter. The circuit diagram of the boost converter-fed BLDC motor drive is shown in Fig. 8. The desired control pulses for the boost converter are generated by the dSPACE1103 controller.

The boost converter is designed using the following equations:

$$\text{Duty cycle} = D = \frac{V_o - V_{in}}{V_o} \tag{10}$$

$$\text{Boost inductor} = L_b = \frac{(1-D)^2\,\text{DR}}{2f} \tag{11}$$

$$\text{Output capacitor} = C_{\min} = \frac{DV_o}{V_r Rf} \tag{12}$$

where D represents the duty cycle, R represents equivalent resistor, f represents switching frequency, V_o represents output voltage, V_{in} represents input voltage, and V_r represents ripple voltage.

A. Forward and Reverse Motoring on the Boost Converter-Embedded BLDC Motor Drive System

Fig. 9 shows the experimental setup of the BLDC motor drive with DC–DC converter. The specifications of the DC–DC boost converter

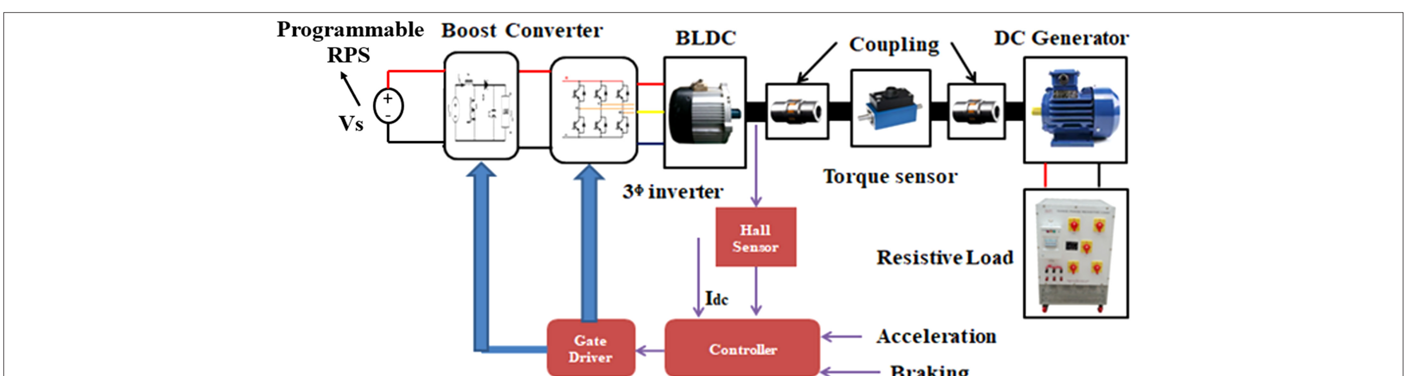

Fig. 7. Block diagram of BLDC drive embedded with DC–DC boost converter.

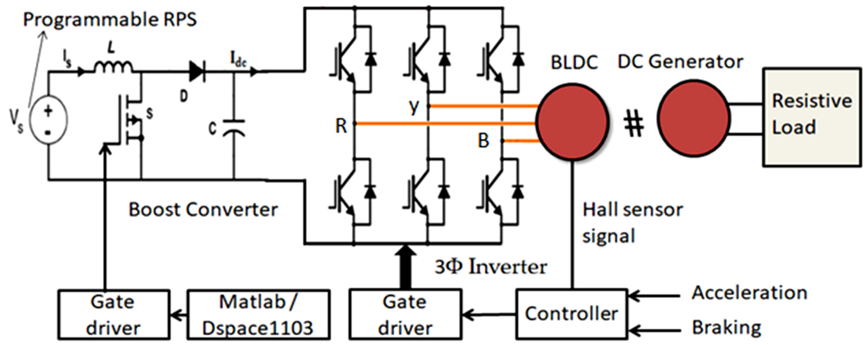

Fig. 8. Circuit diagram of BLDC drive embedded with DC–DC boost converter.

are presented in Table I. The motor runs at no-load at a rated speed of 3000 rpm, and the corresponding voltage and current waveforms with respect to input and output are observed in Fig. 10. The input DC voltage and current are 24.2 V and 5.99 A, respectively. The output current of the boost converter is 3.05 A, the output voltage of the boost converter is 48.13 V, and the switching frequency is 20 kHz.

Fig. 11 shows the overall experimental setup of test-bench arrangements with load conditions. The motor runs at 1500 rpm and electrical loading is added in the DC shunt generator. The input and output voltage values and current values at 2.07 Nm and 2.29 Nm load-torque conditions are presented in Fig. 12(a) and (b); and the values are tabulated in Table V. The simulation results are presented on the left side of each figure and the experimental results are projected on the right side. Both results are in association with each other. The performance of the motor drive is similar to that of the inverter-fed BLDC drive. Instead of a 48 V battery with inverter, a 24 V battery with a boost converter and inverter arrangement is sufficient to minimize the size and cost of the battery. The current drawn from the source is reduced, which minimizes the losses in the power source.

B. Power, Torque, and Speed Characteristics

The DC generator is loaded gradually and the corresponding power, torque, and speed values are measured by a USB torque sensor mounted in the middle of the shaft, which couples both motor and generator. The forward power, torque, and speed characteristics of the BLDC motor with respect to time are drawn in Fig. 13. Initially, the motor runs at 1477 rpm at no-load condition. When the motor is loaded with 2.07 Nm and 2.29 Nm, the corresponding power values are observed and plotted. The performances are the same as those observed in the direct inverter-fed drive system with a 48 V battery. The braking characteristics of the motor are presented in Fig. 14. The motor runs at 1500 rpm and brake is applied at $t=5$ s. The speed of the motor is reduced to zero, and the brake is released at $t=8$ s. The overall efficiency of the boost-converter-fed BLDC motor drive system is calculated by measuring the input power (battery output) and output power (generator). The overall efficiency is 83% and is shown in Table VI.

The performance of the proposed work is compared with the recent literatures [25-29] with respect to the type of the motor and its ratings, battery selection, converter selection, and simulation results, in Table VII. The BLDC motor is used in the research and the results are

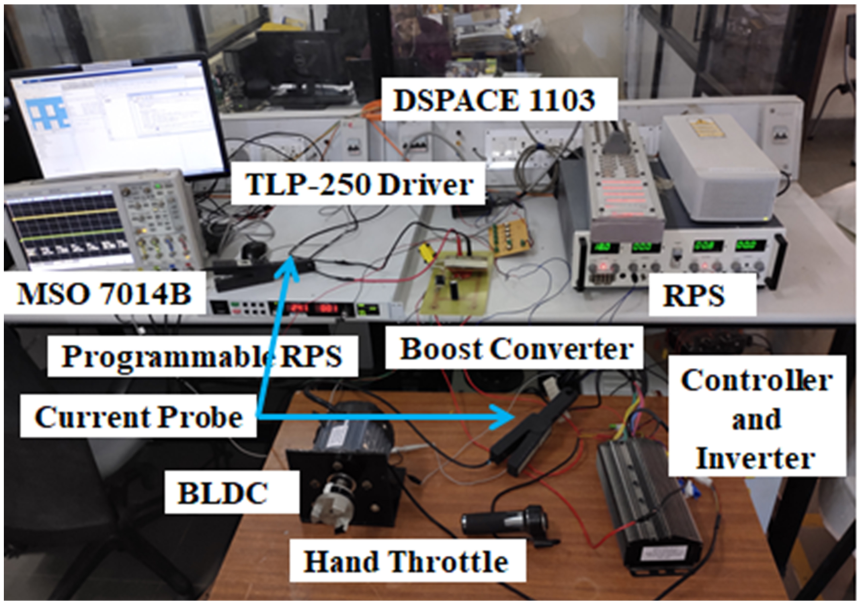

Fig. 9. Experimental setup of BLDC motor drive with DC–DC converter at 3000 rpm.

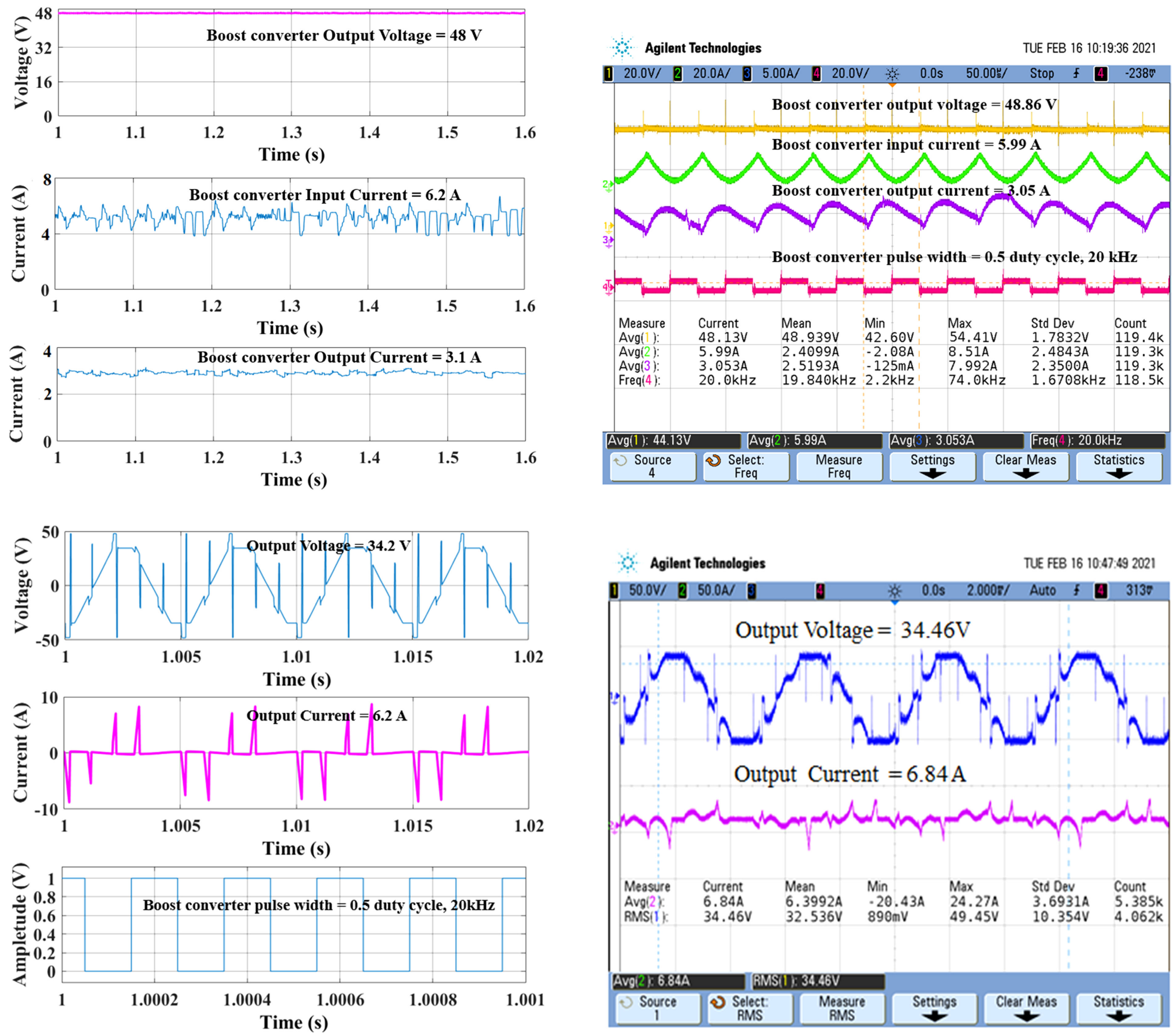

Fig. 10. Voltage and current waveforms with boost converter-embedded BLDC motor drive.

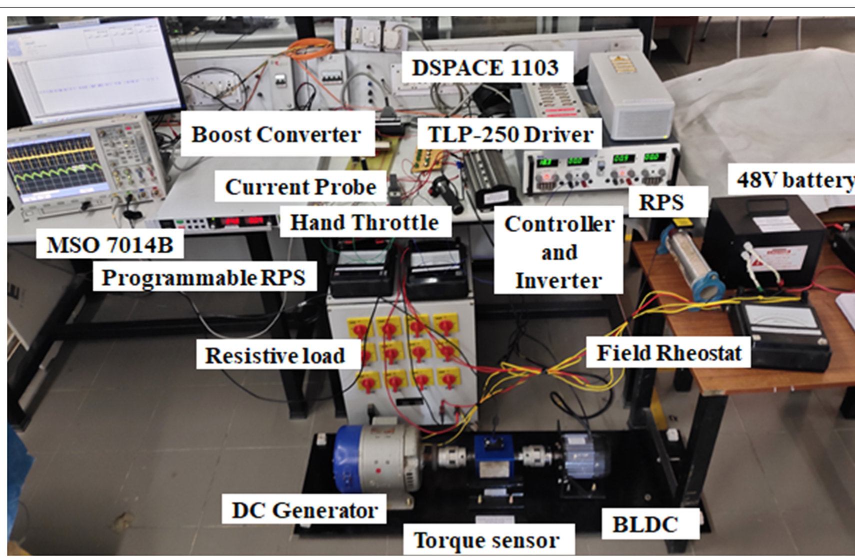

Fig. 11. Experimental setup of the BLDC motor drive with DC–DC converter and DC generator load at 1500 rpm.

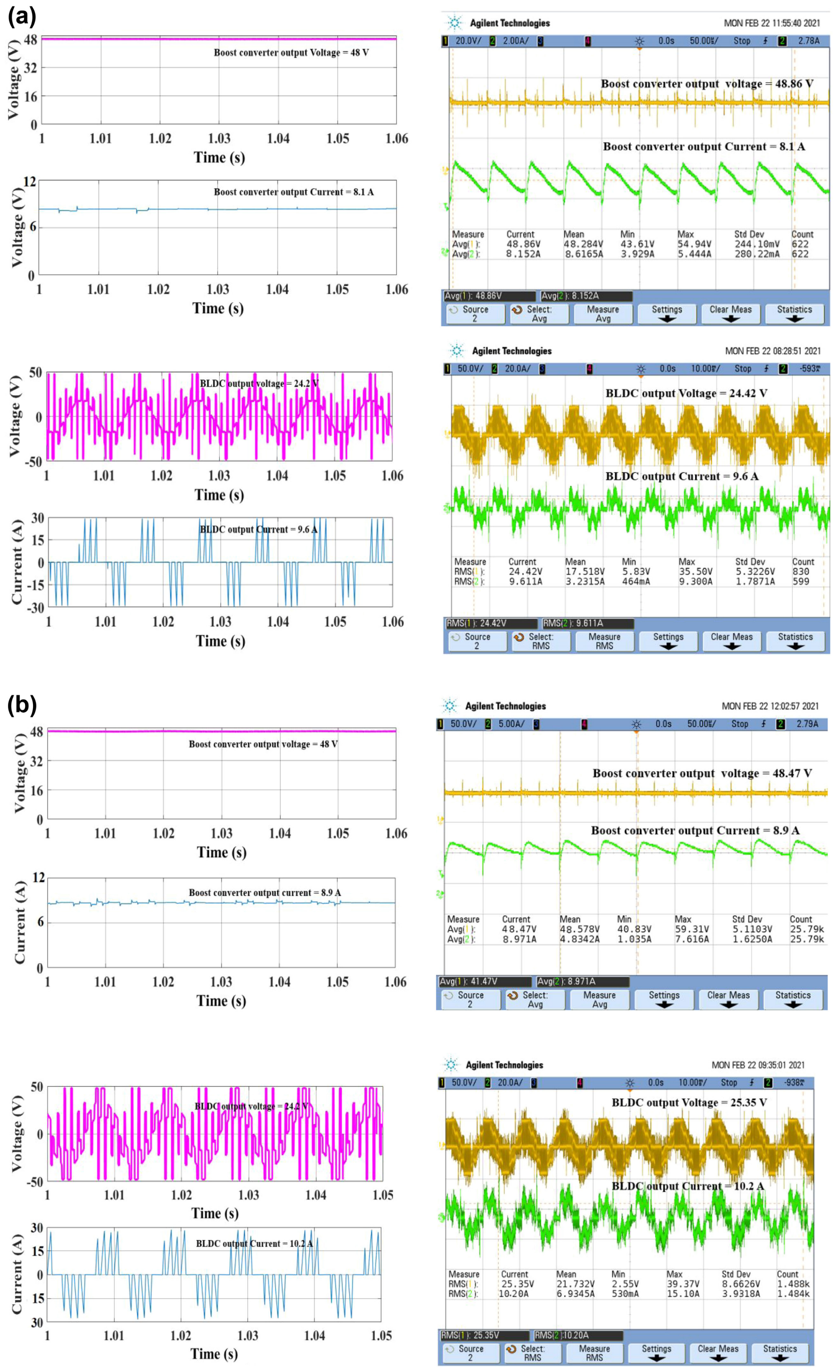

Fig. 12. (a) Waveforms at 2.07 Nm load condition. (b) Waveforms at 2.29 Nm load condition.

TABLE V. LOAD CHARACTERISTICS OF THE DC–DC CONVERTER-EMBEDDED BLDC DRIVE

DC–DC Converter		BLDC Motor		DC Generator				
Output Voltage (V)	Output Current (A)	Output Voltage (V)	Output Current (A)	Field Current (A)	Load Current (A)	Load Voltage (V)	Speed (rpm)	Torque (N m)
48.32	8.01	24.42	9.6	0	1.95	165	1476	2.07
48.32	8.9	25.39	10.2	0.24	2.46	145	1473	2.29

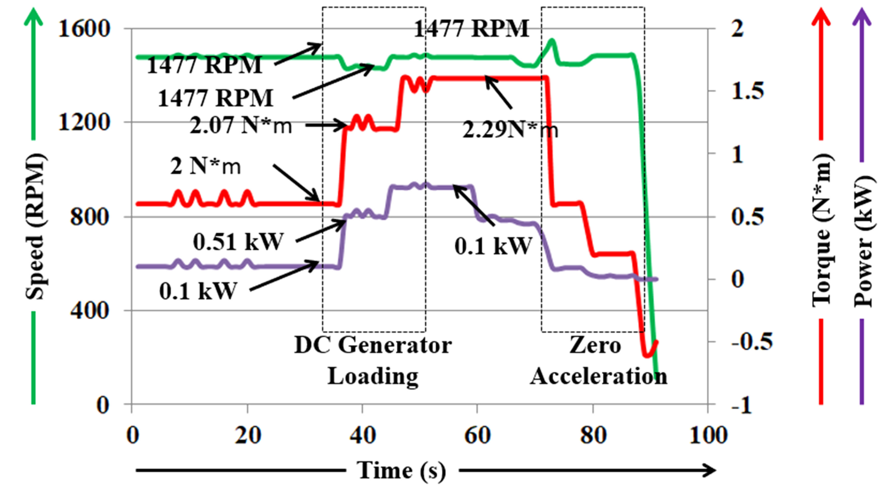

Fig. 13. Speed, torque, and power characteristics plot.

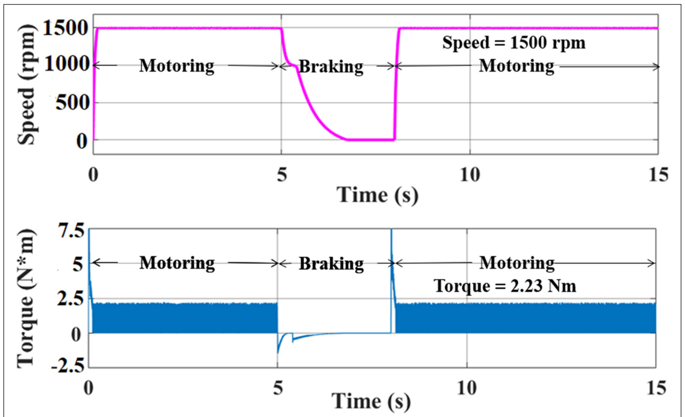

Fig. 14. Boost-converter-fed BLDC motor drive with braking.

TABLE VI. EFFICIENCY OF THE BOOST-CONVERTER-FED DRIVE SYSTEM

Battery Power (W)	BLDC Output Power (W)	Generator Power (W)	Overall Efficiency (%)
387	319.86	321.45	83.06
430	353.95	357.67	83.17

provided only for forward motoring. In the proposed work, the results are discussed under different running conditions with forward and reverse motoring. Both experimental and simulation results are provided for the inverter-fed and boost-converter-fed BLDC motor drives.

IV. CONCLUSION

A detailed discussion on inverter- and DC–DC converter-fed BLDC drive systems with generator loading arrangment is presented. For

TABLE VII. COMPARISON STUDIES ON MOTOR TYPE, BATTERY, CONVERTER, AND SIMULATION RESULTS

References	Input Source	Motor Type	Converter	Simulation Results
[25]	48 V, 4.8 kWh Li-ion battery	48 V, 1 kW, 3000 rpm BLDC motor	Buck converter with PV arrangement	Simulation study was performed at 20 kHz switching frequency. Speed of the motor was presented for forward motoring at 2000 rpm and 500 rpm.
[26]	48 V—LiFePO4 battery	2 kW BLDC hub motor	DC converter not used	The basic characteristics of the BLDC motor such as power–speed, power–torque, and power–current plots were provided.
[27]	60 V, 4 A DC source	60 V, 1 kW BLDC hub motor	DC converter not used	The back emf, gate pulses, and speed waveform for 1000 rpm were presented.
[28]	48 V, 10 A DC source	48 V, 300 W, 2000 rpm BLDC motor	DC converter not used	Speed, torque, and power waveforms were presented. The waveforms were not smooth.
[29]	48 V battery	Not mentioned	Boost converter used	Speed, voltage, and stator current profiles were presented for forward motoring with the dSPACE controller
Proposed	48 V, 24 Ah LiFePO4 battery	48 V, 1 kW, 3000 rpm BLDC motor	Boost converter is added	Speed, torque, and power plots are presented under forward and reverse motoring modes for different speed and torque conditions. Voltage and current waveforms of boost converter and BLDC motor are presented under different operating conditions.

speed, torque, and power measurments, a USB-type torque sensor is mounted in the shaft. The performance analysis is done for the forward- and reverse-motoring modes. The motor output voltage, current, speed, torque, and power are noted for both modes under different running conditions. A DC–DC converter is employed to reduce the battery voltage and it is operated in closed-loop control for constant voltage operation. Simulation and experimental results are presented to validate the performance of the drive system. A DC–DC converter with a low-voltage battery is a good choice for EV applications. The overall efficiency of the drive system is 83% in both the inverter- and the DC–DC converter-fed drive systems. Conventionally, in a battery-operated vehicle, the system design cost decreases with maximum energy utilization. The analysis will be very useful for new researchers in the EV domain, for a basic idea on forward and reverse motoring with inverter- and DC–DC converter-fed BLDC motor drives. The low-voltage battery can be charged easily under regenerative braking for different speed conditions.

Peer-review: Externally peer-reviewed.

Author Contributions: Concept – R.A, R.G.; Design – R.A, R.G.; Supervision – R.G.; Materials – R.A.; Data Collection and/or Processing – R.A.; Analysis and/or Interpretation – R.A, R.G.; Literature Search – R.A.; Writing Manuscript – R.A, R.G.; Critical Review – R.G.

Acknowledgments: The authors sincerely thank the School of Electrical Engineering, Vellore Institute of Technology, Chennai for providing the seed fund to carry out this research study with an experimental setup.

Conflict of Interest: The authors have no conflicts of interest.

Financial Disclosure: The research was supported by Vellore Institute of Technology – Chennai (Seed fund).

REFERENCES

1. Available: https://en.wikipedia.org/wiki/Electric_car_use_by_country.
2. S. Kim and S. H. Choi, *Development of Fuel Cell Hybrid Vehicle by Using Ultra-Capacitors as a Secondary Power Source*. Detroit, MI: society of American engineers World Congress, 2005.
3. L. Gao, R. A. Dougal, and S. Liu, "Power enhancement of an actively controlled battery/ultracapacitor hybrid," *IEEE Trans. Power Electron.*, vol. 20, no. 1, pp. 236–243, Jan. 2005. [CrossRef]
4. W. Lhomme, P. Delarue, P. Barrade, A. Buoscayrol, and A. Rufer, "Design and control of a supercapacitor storage system for traction applications," in *IEEE Ind. Appl. Conference*. Kowloon, Hong Kong, Oct. 2005, pp. 2013–2020.
5. L. Solero, A. Lidozzi, and J. A. Pomilio, "Design of multiple-input power converter for hybrid vehicles," *IEEE Trans. Power Electron.*, vol. 20, no. 5, pp. 1007–1016, Sep. 2005. [CrossRef]
6. Z. Jiang and R. A. Dougal, "A compact digitally controlled fuel cell/battery hybrid power source," *IEEE Trans. Ind. Electron.*, vol. 53, no. 4, pp. 1094–1104, Jun. 2006. [CrossRef]
7. S. M. Lukic, S. G. Wirashanga, F. Rodriugez, C. Jian, and A. Emadi, "Power management of an ultracapacitor/battery hybrid energy storage system in an HEV," in *IEEE Vehicle Power and Propulsion Conference*, Windsor, United Kingdom, 2006, pp. 1–6.
8. M. Ortuzar, J. Moreno, and J. Dixon, "Ultracapacitor-based auxiliary energy system for an electric vehicle: implementation and evaluation," *IEEE Transactions on Industrial Electronics*, vol. 54, no. 4, pp. 2147–2156, Aug. 2007.
9. S. M. Lukic, J. Cao, R. C. Bansal, F. Rodriguez, and A. Emadi, "Energy storage systems for automotive applications," *IEEE Trans. Ind. Electron.*, vol. 55, no. 6, pp. 2258–2267, June 2008. [CrossRef]
10. J. Cao and A. Emadi, "A new battery/ultracapacitor hybrid energy storage system for electric, hybrid, and plug-in hybrid electric vehicles," *IEEE Trans. Power Electron.*, vol. 27, no. 1, pp. 122–132, May 2011.
11. C. Zheng, T. Zahid, K. Xu, X. Zhang, and G. Xu, "Fully electrified regenerative braking control for deep energy recovery and maintaining safety of electric vehicles," *IEEE Trans. Veh. Technol.*, vol. 65, no. 3, pp. 1186–1198, 2015.
12. K. Itani, A. De Bernardinis, Z. Khatir, A. Jammal, and M. Oueidat, "Regenerative braking modeling, control, and simulation of a hybrid energy storage system for an electric vehicle in extreme conditions," *IEEE Trans. Transp. Electrif.*, vol. 2, no. 4, pp. 465–479, 2016. [CrossRef]
13. F. Naseri, E. Farjah, and T. Ghanbari, "An efficient regenerative braking system based on battery/supercapacitor for electric, hybrid, and plug-in hybrid electric vehicles with BLDC motor," *IEEE Trans. Veh. Technol.*, vol. 66, no. 5, pp. 1–1, 2017. [CrossRef]
14. X. Zhang, D. Gohlich, and J. Li, "Energy-efficient toque allocation design of traction and regenerative braking for distributed drive electric vehicles," *IEEE Trans. Veh. Technol.*, vol. 67, no. 1, pp. 285–295, 2018. [CrossRef]
15. H. Peng, J. Wang, W. Shen, D. Shi, and Y. Huang, "Controllable regenerative braking process for hybrid battery–ultracapacitor electric drive systems," *IET Power Electron.*, vol. 11, no. 15, pp. 2507–2514, 2018. [CrossRef]
16. W. Li, H. Du, and W. Li, "Driver intention-based coordinate control of regenerative and plugging braking for electric vehicles with in-wheel PMSMs," *IET Intell. Transp. Syst.*, vol. 12, no. 10, pp. 1300–1311, 2018. [CrossRef]
17. Y. Yuan, J. Zhang, Y. Li, and C. Li, "A novel regenerative electrohydraulic brake system: development and hardware-in-loop tests," *IEEE Trans. Veh. Technol.*, vol. 67, no. 12, pp. 11440–11452, 2018. [CrossRef]
18. B. Liu, L. Li, X. Wang, and S. Cheng, "Hybrid electric vehicle downshifting strategy based on stochastic dynamic programming during regenerative braking process," *IEEE Trans. Veh. Technol.*, vol. 67, no. 6, pp. 4716–4727, 2018. [CrossRef]
19. J. Wang and R. He, "Varying charge voltage in the steps control method of ABS for in- wheel motors driven electric vehicles based on an improved LQG scheme," *IEEE Access*, vol. 6, pp. 15039–15050, 2018. [CrossRef]
20. S. Heydari, P. Fajri, Md. Rasheduzzaman, and R. Sabzehgar, "Maximizing regenerative braking energy recovery of electric vehicles through dynamic low-speed cut-off point detection," *IEEE Trans. Transp. Electrif.*, vol.5, no.1, pp. 261–271, Mar. 2019.
21. D. Pi, Q. Cheng, B. Xie, H. Wang, and X. Wang, "A Novel pneumatic brake pressure control algorithm for regenerative braking system of electric commercial trucks," *IEEE Access*, vol. 7, pp. 83372–83383, 2019. [CrossRef]
22. S. Heydari, P. Fajri, R. Sabzehgar, and A. Asrari, "Optimal brake allocation in electric vehicle for maximizing energy harvesting during braking," *IEEE Trans. Energy Convers.*, vol. 35, no. 4, pp. 1806–1814, Dec. 2020. [CrossRef]
23. Z. Ma and D. Sun, "Energy recovery strategy based on ideal braking force distribution for regenerative braking system of a four-wheel drive electric vehicle," *IEEE Access*, vol. 8, p. 136234–136242, 2020. [CrossRef]
24. Y. Yang, Q. Tang, L. Bolin, and C. Fu, "Dynamic coordinated control for regenerative braking system and anti-locking braking system for electrified vehicles under emergency braking conditions," *IEEE Access*, vol. 8, pp. 172664–172677, 2020. [CrossRef]
25. I. Haldar, D. Debnath, and T. R. Choudhury, "Design of a battery charger fed from two solar panels arranged at different inclination for E-Rickshaw and DC microgrid applications," in *1st International Conference on Power Electronics and Energy (ICPEE)*. IEEE Publications, 2021, pp. 1–6.
26. G. Udupa, J. Freeman, V. Nimbewal, R. K. Choudhary, S. Sasikumar, and S. V. Nair, "Design and manufacture of Amrita Surya Vahini—a solar auto rickshaw," in *International Conference on Robotics and Automation for Humanitarian Applications (RAHA)*. IEEE Publications, 2016, pp. 1–6.
27. P. V. Sidharthan and Y. Kashyap, "Brushless DC hub motor drive control for electric vehicle applications," in *2020 First International Conference on Power, Control and Computing Technologies (ICPC2T)*. IEEE Publications, 2020, pp. 448–453.
28. M. A. Akhtar, Md. Musraph Hussain, P. S. Pal, and S. Saha, "dSPACE based motor testing platform for characterization of BLDC motor performance under different loading conditions," in *8th IEEE India International Conference on Power Electronics (IICPE)*. IEEE Publications, 2018, pp. 1–6.
29. Y. Kumar, D. Varaprasanna, A. Kumar, B. V. Ravi Kumar, and S. Karunanidhi, "An energy efficient drive configuration using closed loop boost DC-DC converter for an electric vehicle," in *IEEE Transp. Electrif. Conference (ITEC-India)*. IEEE Publications, 2019, pp. 1–4.

Mr. R. Amalrajan obtained his B.E. degree in Electrical and Electronics Engineering from Adhiparasakthi College of Engineering, affiliated to Anna University, Tamil Nadu in 2012. He pursued his M.Tech. in Power Electronics and Drives from Sree Sastha Institute of Engineering and Technology, affiliated to Anna University, in 2016. He is currently pursuing his Ph.D. at the School of Electrical Engineering, Vellore Institute of Technology-Chennai, in Tamil Nadu, India. He has published 2 research papers in reputed journals and presented 2 papers in international conferences. His research interests are in the areas of BLDC motor drives and power electronics converters.

Dr. R. Gunabalan obtained his B.E. in Electrical and Electronics Engineering from Manonmanium Sundaranar University, Tirunelveli, Tamil Nadu in 2000 and M.Tech. in Electrical Drives and Control from Pondicherry University in 2006. He pursued his Ph.D. at Anna University, Chennai, in Tamil Nadu, India in 2015. He is working as an Associate Professor in the School of Electrical Engineering, Vellore Institute of Technology-Chennai, in Tamil Nadu, India. He has published 25 research papers in reputed journals and presented around 25 papers in national and international conferences. His research interests are in the areas of DC–DC power converters and the estimation and control of induction motor drives. He is a life-member of ISTE and IEI and a member of IEEE.